


## Research Article

# Allicin-Mediated Cell Cycle Regulation Reverses Taxol Resistance in NSCLC: Molecular Insights and Therapeutic Potentia

Xudong Gao <sup>1</sup>, Ramesh kumar Santhanam <sup>2</sup>, Zeng Huang,<sup>3</sup> Mingyue Liu,<sup>4</sup> Shanbo Hou,<sup>5</sup> Aigang Song,<sup>5</sup> Tianshu Ren <sup>1</sup> and Qingchun Zhao <sup>1</sup>

<sup>1</sup>Department of Pharmacy, General Hospital of Northern Theater Command, Shenyang, China

<sup>2</sup>Faculty of Science and Marine Environment, Universiti Malaysia Terengganu, Kuala Nerus, Terengganu, Malaysia

<sup>3</sup>Wuya College of Innovation, Shenyang Pharmaceutical University, Shenyang, China

<sup>4</sup>Weifang People's Hospital, Weifang, China

<sup>5</sup>Luoxin Pharmaceuticals Group Stock Co., Ltd., Linyi, China

Correspondence should be addressed to Tianshu Ren; sz\_pharm@163.com and Qingchun Zhao; zhaoqingchun1967@163.com

Received 5 August 2023; Revised 22 September 2023; Accepted 27 September 2023; Published 13 December 2023

Academic Editor: Nadica Maltar Strmečki

Copyright © 2023 Xudong Gao et al. This is an open access article distributed under the Creative Commons Attribution License, which permits unrestricted use, distribution, and reproduction in any medium, provided the original work is properly cited.

The clinical efficacy of non-small-cell lung cancer (NSCLC) treatment is significantly hindered by Taxol resistance, demanding the exploration of novel approaches to overcome this challenge. Natural products, renowned for their diverse anticancer potential, offer hope, with allicin emerging as a captivating contender. However, the intricate role and underlying mechanisms of allicin in NSCLC Taxol resistance remain largely unexplored. In this extensive investigation, we delve into the impact of allicin on Taxol resistance, meticulously examining both *in vitro* and *in vivo* scenarios. Remarkably, allicin effectively curbs the proliferation and migration of A549/Taxol cells while inducing apoptosis. Unraveling the regulatory potential of genes like CDK1 in the cell cycle pathway, allicin demonstrated the ability to arrest cells in the G2/M phase, thus disrupting the cell cycle and heightening Taxol sensitivity. Strikingly, when combined with Taxol, allicin showed the ability to promote Taxol to inhibit tumor growth and reduce lung nodules in tumor-bearing mice, all without significant toxicity. Importantly, allicin's prowess in reversing Taxol resistance *via* cell cycle regulation sheds light on its potential as a resistance-reversing agent in NSCLC, marking a vital milestone in the quest for natural source therapies.

## 1. Introduction

Non-small cell lung cancer (NSCLC) is one of the most common cancers globally and has the highest mortality rate among all cancer types [1, 2]. Taxol is a diterpene alkaloid chemical that is derived from natural sources and exhibits strong anticancer properties. It serves as the first-line chemotherapeutic treatment for NSCLC. Taxol has a powerful ability to kill tumor cells, but as primary or acquired drug resistance develops in tumor cells, its effectiveness as a treatment is severely compromised [3, 4]. This puts patient survival and treatment rates at risk and severely restricts the use of Taxol in clinical settings. Therefore, before the

development of new and more potent chemotherapy medications, increasing the sensitivity of currently available chemotherapy treatments and combating drug resistance to chemotherapy drugs are the primary strategies to increase the efficacy of chemotherapy.

Natural products have chemical diversity, rich biological activity, multi-target action ability, low side effects, and good safety. In addition, the sustainability and accessibility of natural products also make them a strong candidate for finding new drug resistance reversal drugs. Allicin is a sulfur compound extracted from garlic, which has a variety of active ingredients [5]. It has a wide range of biological activities, including antibacterial, anti-inflammatory, and

antitumor effects [5–7]. This makes allicin a potential compound for reversing paclitaxel resistance research. In recent years, allicin has been found to increase drug sensitivity in combination with cisplatin, 5-fluorouracil, and other antitumor drugs, but the mechanism is still unclear [8, 9].

In this study, high-throughput sequencing was used to compare the transcriptome information of drug-resistant cells and sensitive cells, which can find possible changes in gene expression during drug resistance, to identify potential drug-resistant genes; furthermore, by analyzing the mRNA sequencing data of drug-resistant cells treated with allicin, a new reversal targets can be discovered. The study aims to explore the effects of allicin in reversing Taxol resistance in NSCLC through *in vitro* and *in vivo* experiments. It is of great significance in the study of natural products reversing drug resistance, which is conducive to identifying drug resistance genes, discovering new reversal targets, and revealing the reversal mechanism, and provides an experimental basis and theoretical basis for an in-depth understanding of natural products reversing drug resistance.

## 2. Materials and Methods

**2.1. Materials and Chemicals.** Allicin injection (10 mL: 30 mg) was sponsored by Cisen Pharmaceutical Co., Ltd. (Shandong, China). Taxol injection (5 mL: 30 mg) was obtained from Beijing SL Pharmaceutical Co., Ltd. (Beijing, China). MTT (3-(4,5-dimethylthiazol-2-yl)-2,5-diphenyltetrazolium bromide) and TRIzol reagent (Ambion) were obtained from Sigma-Aldrich (Shanghai) Trading Co., Ltd. (Shanghai, China). RPMI 1640 and fetal bovine serum (FBS) were obtained from Biological Industries Ltd. and IATI (Israel Advanced Technology Industries). PBS buffer was obtained from Solarbio (Beijing, China). Trypsin was obtained from Gibco Life Technologies (New York, USA). Penicillin-streptomycin solution was purchased from HyClone Co. (Utah, USA). All other chemicals and reagents were purchased locally and were of analytical grade.

**2.2. Cell Culture.** Human non-small-cell lung cancer cells (A549 cells) and Taxol-resistant A549 (A549/Taxol) cells were obtained from Shanghai Meixuan Biotechnology Co., Ltd. (Shanghai, China), and they were cultured in T25 flasks at 37°C in a 5% CO<sub>2</sub> atmosphere. According to our previous study, the IC<sub>50</sub> of Taxol on A549 and A549/Taxol cells was 1.20 nM and 470.60 nM, respectively, and the drug-resistance index (RI) of A549/Taxol cells was 403.4. All cells were maintained in RPMI 1640 medium supplemented with 10% heat-inactivated fetal bovine serum (FBS), 100 U/mL of penicillin, and 100 µg/mL of streptomycin.

**2.3. MTT Assay.** MTT assay was conducted to assess cell viability [3]. A549/Taxol cells were cultured in 96-well plates at  $8 \times 10^3$  cells/well density and treated with various allicin concentrations (1–1000 µM) for 48 hours. The nontoxic concentration of allicin, inhibiting cell growth by less than 10%, was determined. Subsequently, A549/Taxol cells were

cotreated with allicin (IC<sub>10</sub>) and 300 nM Taxol for 48 hours. The absorbance reading was measured at 490 nm, and the reversal fold (RF) was calculated as  $RF = (IC_{50} \text{ of Taxol}) / (IC_{50} \text{ of combination})$ . This study aimed to explore the potential of allicin in reversing Taxol resistance in A549/Taxol cells.

**2.4. Cell Colony Formation Assay.** A549/Taxol cells in the logarithmic growth phase were seeded in 6-well plates with  $1.0 \times 10^3$  cells per well [1]. The cells were treated with half of IC<sub>10</sub>, IC<sub>10</sub>, and twice IC<sub>10</sub> allicin for 24 h, and then the cells were replaced with drug-free medium and incubated for another 10 days. Then, the colonies were fixed with methanol for 20 min and then stained with 0.1% (*w/v*) crystal violet for 30 min. Finally, the colonies were washed three times with PBS, dried naturally, and photographed. ImageJ software was used to count the number of clones.

**2.5. Wound-Healing Assay.** The wound-healing assay was used to evaluate the effect of allicin combined with Taxol on the migration ability of A549/Taxol cells [1]. Cells were seeded into six-well plates at a density of  $2.0 \times 10^5$  and incubated overnight. A 200 µL pipette tip was used to scrape a straight line across the monolayer of cells at the bottom of the six-well plate. Cells were treated with 5, 10, and 20 µM allicin and 300 nM Taxol. Images were acquired at 0, 24, and 48 h, respectively. The average scratch width was calculated and compared with the scratch width at 0 h. The relative mobility of cells in each group at 24 and 48 h was calculated to evaluate the scratch repair ability.

**2.6. Hoechst 33342 Staining.** Hoechst 33342 staining was used to evaluate the effect of allicin combined with Taxol on the apoptosis of A549/Taxol cells [4]. The cells were washed twice with precooled PBS, then stained in the dark with Hoechst 33342 solution for 15 minutes, and then imaged using a fluorescence inversion microscope (Olympus Corp., Tokyo, Japan). After Hoechst 33342 staining, normal and necrotic cells showed weak blue fluorescence, while apoptotic cells showed strong blue fluorescence.

**2.7. RNA Sequencing.** The experiment included three groups: A549 sensitive cells, A549/Taxol-resistant cells, and A549/Taxol cells treated with allicin (at IC<sub>10</sub> concentration). Total RNA was extracted using the TRIzol method, and its integrity was verified with the RNA Nano 6000 test kit on the Agilent 2100 Bioanalyzer [10]. The transcriptome sequencing was carried out by Shanghai Personalbio Biotechnology Co., Ltd. The mRNA was enriched using oligo (dT) magnetic beads, fragmented to approximately 300 bp, and used for cDNA synthesis with random primers and reverse transcriptase. The library was constructed, and PCR amplification enriched the fragments. Library quality was checked using the Agilent 2100 Bioanalyzer, and libraries with different index sequences were mixed accordingly. The mixed library was diluted to 2 nM, and single-strand libraries were formed through alkali denaturation. Samples

were sequenced using the Illumina sequencing platform and Next Generation Sequencing (NGS). Raw data underwent filtering to ensure data quality and minimize interference from invalid data during information analysis.

**2.8. GO and KEGG Enrichment Analysis.** The differences in gene expression between two different groups were analyzed using DESeq2 software package:  $|\log_2\text{FoldChange}| > 1$ ,  $P$  value  $< 0.05$ , FDR  $< 0.05$ . The Gene Ontology (GO) and the Kyoto Encyclopedia of Genes and Genomes (KEGG) were used to analyze DEGs' molecular function, cell composition, biological process, and related signal pathways [11]. Fisher test assessed pathway enrichment with  $P < 0.05$  as the threshold for significant enrichment compared to the whole genome background.

**2.9. Allicin Reversed Taxol Resistance in A549/Taxol Cells through G2/M Phase Arrest.** PPI network showed that CDK1, CCNA2, CCNB1, CCNB2, CDC20, and other genes were essential in allicin reversal of Taxol resistance, and these genes were closely related to the cell cycle. GO enrichment and KEGG pathway analysis also revealed the importance of cell cycle. Therefore, flow cytometry and western blotting were used to investigate the effect of allicin at IC<sub>10</sub> concentration on the cell cycle of A549/Taxol cells.

**2.9.1. Cell Cycle Assay.** Cells were seeded in 6-well plates at a density of  $1 \times 10^6$  cells/well. When the degree of cell confluence was 60–70%, the cells were treated with allicin (5, 10, and 20  $\mu\text{M}$ ) combined with Taxol (300 nM) for 24 h [12]. The cells were collected and prepared into a single cell suspension according to the manufacturer's instructions, fixed in 70% cold ethanol at  $-20^\circ\text{C}$  overnight, washed twice with precooled PBS, and stained with PI for 15 min. The flow cytometry analysis was performed using a FACS Verse flow cytometer (BD Biosciences, San Jose, CA) with cell counts of 10,000. FlowJO software (Treestar, Ashland, OR) was used to analyze data.

**2.9.2. Western Blotting.** Prepared cell lysates and determined the protein content using the BCA protein assay kit [3]. After blocking with 5% BSA, the membrane was incubated with primary antibodies against  $\beta$ -actin, CDK1, cyclin B1, and p21 at  $4^\circ\text{C}$  overnight. Then, the membrane was incubated with an IgG secondary antibody (1 : 5000) at room temperature for 1 hour. Ultrasensitive ECL chemiluminescence reagent was used to display protein bands, and an enhanced chemiluminescence system (Bio-Rad imaging system, USA) was used for observation. The loading control was  $\beta$ -actin. Densitometric analysis was performed using the ImageJ software (National Institute of Health, MD).

**2.10. The Activity of Allicin in Reversing Taxol-Resistance In Vivo**

**2.10.1. Establishment of the Nude Mouse Orthotopic Tumor Model of Taxol-Resistant Human Non-Small-Cell Lung Cancer.** Male BALB/c nude mice (4–6 weeks, 18–22 g) from

Beijing Weitong Lihua Laboratory Animal Technology Co., Ltd., were housed in an SPF environment. A549/Taxol cells ( $1.0 \times 10^7/\text{mL}$ ) were injected (50  $\mu\text{L}$ ) into the tail vein of each mouse. After 7 days, tumor-bearing mice were divided into five groups: blank, negative control (saline), Taxol (10 mg/kg), allicin (5 mg/kg), and allicin + Taxol (5 mg/kg + 10 mg/kg). Drugs were administered every two days *via* intraperitoneal injection. Body weight was measured daily. After 15 days, mice were sacrificed, lung tissue was fixed with Bouin solution, and it was stored for subsequent experiments.

**2.10.2. Hematoxylin-Eosin (H&E) Staining.** H&E staining (using the Beyotime C0105S kit) was performed to evaluate allicin's effect on reversing Taxol resistance in A549 cells [13]. Paraffin sections were dewaxed twice with xylene for 10 minutes each time, then gradually rehydrated with 100–70% ethanol, and then immersed in deionized water. Furthermore, nuclei were stained with 10% hematoxylin for 5 minutes, and the cytoplasm was counterstained with eosin for 2 minutes. After dehydration and sealing with neutral gum, the slices were observed and photographed under an inverted microscope, carefully avoiding bubbles in the process.

**2.10.3. Immunohistochemistry Analysis.** Paraffin sections of tumor tissue were prepared as mentioned earlier. Antigen repaired was performed by boiling the sections in 10 mM sodium citrate buffer (pH 6.0). To reduce nonspecific background staining, sections were treated with hydrogen peroxide block and 10% goat serum. CDK1, cyclin B1, and p21 antibodies were incubated overnight, followed by biotin-labeled secondary antibodies. DAB chromogenic Kit was used for visualization, and Mayer's hematoxylin was used for counterstaining. Digital images were captured using Keyence BZ-X700 microscopes and BZ-X analyzer software (Osaka, Japan).

**2.11. Statistical Analysis.** All data were represented as mean  $\pm$  SD. Data analysis were performed using one-way ANOVA followed by a Dunnett test in GraphPad prism software (Version 5). An unpaired Student's *t*-test was used to compare the difference between the two experimental groups.  $P < 0.05$  were considered statistically significant.

### 3. Results

**3.1. Effect of Allicin on Proliferation and Migration of A549/Taxol Cells.** In our previous study [4], the drug resistance index of A549/Taxol cells was 403.4, indicating significant Taxol resistance. MTT assay, cell colony formation assay, and cell wound-healing assay were used to evaluate the effect of allicin on the proliferation and migration of A549/Taxol cells. Allicin showed concentration- and time-dependent inhibition of A549/Taxol cell proliferation (Figure 1(a)). The IC<sub>50</sub> values at 24 h, 48 h, and 72 h were 94.83  $\mu\text{M}$ , 60.02  $\mu\text{M}$ , and 38.28  $\mu\text{M}$ , respectively, while the IC<sub>10</sub> values

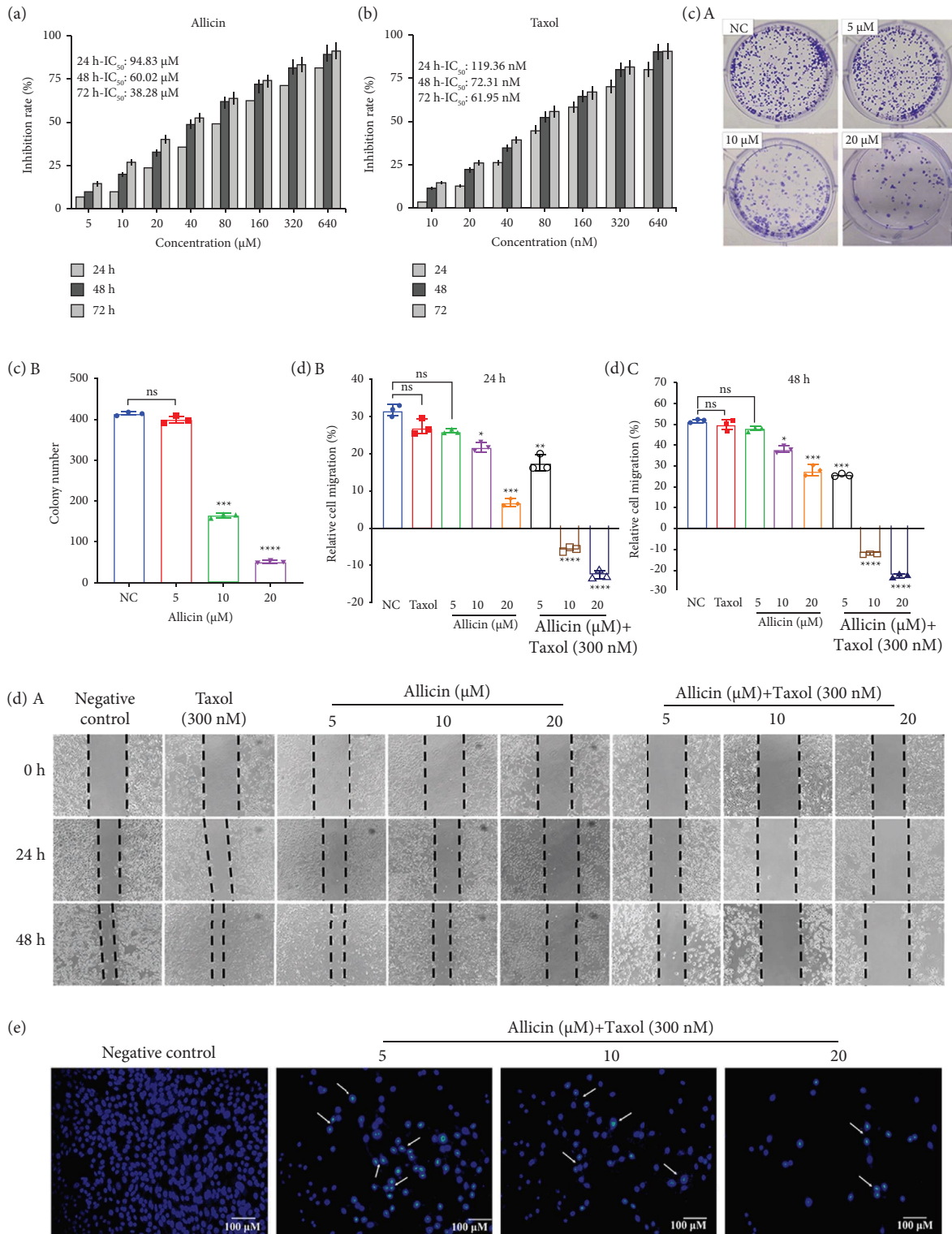


FIGURE 1: Effects of allicin on proliferation and migration of A549/Taxol cells. (a) The inhibition rate of allicin at different concentrations on A549/Taxol cells was detected by MTT assay at 24, 48, and 72 hours of treatment; (b) the inhibition rates of different concentrations of Taxol combined with allicin ( $IC_{10}$ ) on A549/Taxol cells was detected by MTT assay at 24, 48, and 72 h; (c) representative Images (A) and statistical analysis (B) of colony formation in A549/Taxol cells with different concentrations of allicin combined with Taxol (300 nM); (d) wound healing assay was performed in A549/Taxol cells with different concentrations of allicin combined with Taxol (300 nM) at for 0, 24, and 48 h, respectively; representative images (A) and statistical analysis (B, C). (e) Hoechst 33342 staining results for 48 h in A549/Taxol cells. Strong blue fluorescence indicated apoptotic cells, scale bar = 100 μm. The data were expressed as mean ± SD, compared with the negative control group,  $P < 0.05$ ,  $**P < 0.01$ ,  $***P < 0.001$ .

at these time points were 10.09  $\mu\text{M}$ , 6.17  $\mu\text{M}$ , and 3.49  $\mu\text{M}$ . When treated with IC<sub>10</sub> allicin combined with 300 nM Taxol for 24 h, 48 h, and 72 h, the IC<sub>50</sub> of Taxol decreased to 119.36 nM, 72.31 nM, and 61.95 nM, respectively, indicating a significant reversal of drug resistance with fold values of 3.94, 6.51, and 7.60 (Figure 1(b)).

The long-term inhibitory effect of allicin on Taxol-induced proliferation of A549/Taxol cells was assessed by colony-forming assay. In the negative control group (NC), 418 cell colonies were formed after 10 days of culture. Treatment with allicin (5, 10, and 20  $\mu\text{M}$ ) led to a significant reduction in the number of cell colonies: 389, 165, and 55 colonies, respectively. The decrease in cell colony formation was more pronounced with higher allicin concentrations, indicating allicin's ability to enhance Taxol inhibition and reverse Taxol resistance in A549/Taxol cells (Figure 1(c)).

The invasion and metastasis of lung cancer is a complex biological process in clinic. Therefore, we investigated the effects of allicin combined with Taxol on the migration ability of A549/Taxol cell line at different concentrations and times. As shown in Figure 1(d), cell migration can be observed through wound-healing assay [14]. The relative migration rates of A549/Taxol cells in the negative control group and 5, 10, and 20  $\mu\text{M}$  allicin combined with 300 nM Taxol group at 24 h were 35.52%, 20.93%, -1.21%, and -8.93%, respectively. The relative mobility at 48 h was 52.80%, 27.59%, 3.17%, and -20.15%. Previous results have shown that allicin combined with Taxol can promote apoptosis in NSCLC cells. Therefore, Hoechst 33342 staining was used to detect cell morphology and apoptosis in each group. We observed chromatin pyknosis, nuclear reduction, and intense blue fluorescence in A549/Taxol cells. The results suggest that allicin combined with Taxol may inhibit the invasion and metastasis of tumor by inhibiting the migration of tumor cells (Figure 1(e)).

The invasion and metastasis of lung cancer is a complex biological process in clinic. Therefore, we investigated the effects of allicin combined with Taxol on the migration ability of A549/Taxol cell line at different concentrations and times. As shown in Figure 1(d), cell migration can be observed through wound-healing assay [14]. The relative migration rates of A549/Taxol cells in the negative control group and 5, 10, and 20  $\mu\text{M}$  allicin combined with 300 nM Taxol group at 24 h were 35.52%, 20.93%, -1.21%, and -8.93%, respectively. The relative mobility at 48 h was 52.80%, 27.59%, 3.17%, and -20.15%. Previous results have shown that allicin combined with Taxol can promote apoptosis in NSCLC cells. Therefore, Hoechst 33342 staining was used to detect cell morphology and apoptosis in each group. We observed chromatin pyknosis, nuclear reduction, and intense blue fluorescence in A549/Taxol cells. The results suggest that allicin combined with Taxol may inhibit the invasion and metastasis of tumor by inhibiting the migration of tumor cells (Figure 1(e)).

**3.2. Effects of Taxol and Allicin on Gene Expression in A549 Cells or A549/Taxol Cells.** The gene expression was standardized using the counts per million algorithm, and

DESeq2 was used to identify DEGs based on  $|\log_2(\text{fold change, FC})| > 1$  and  $\text{FDR} < 0.05$  [15]. Genes with  $\log_2 \text{FC} > 1$  and  $\text{FDR} < 0.05$  were considered "Up" (upregulated), while those with  $\log_2 \text{FC} < 1$  and  $\text{FDR} < 0.05$  were considered "Down" (downregulated). The remaining data were classified as "Not DEG" (not significantly differentially expressed genes). The statistical results of DEG between different groups are as follows: A (A549 group) vs. AT (A549/Taxol group): 5866 genes (3313 up, 2553 down); A vs. ATA (A549/Taxol treated with allicin group): 6170 genes (3412 up, 2764 down); AT vs. ATA: 480 genes (123 up, 357 down).

In addition, the volcano plot could directly show the difference of genes between different groups [16]. As shown in Figures 2(a)~2(c), The two dotted lines indicated the  $\log_2(\text{FC})$  positions, with blue points representing downregulated genes and red points representing upregulated genes compared to the control. The closer the point to the end, the greater the difference. Hierarchical clustering was performed on DEGs, and the results were presented as heat maps (Figures 2(d)~2(g)). Genes with similar expression patterns likely share common functions and participate in common metabolic and signaling pathways.

Venn diagrams and UpSet diagrams were used to display the sets of DEGs compared between groups [17]. The overlapping part represented gene sets jointly regulated across different treatments, while the separate parts represented genes specifically regulated under certain treatments. In Figures 2(h)~2(i), there were 310 common DEGs in the three groups, which were considered the core genes of allicin-reversing Taxol resistance in A549/Taxol cells. Among them, 38 genes were commonly upregulated, 176 were commonly downregulated, and 96 showed different regulatory patterns in different groups. Comparing WITH to ATA, there were 53 upregulated genes and 257 downregulated genes.

### 3.3. Biological Function of Target and Target Pathway Analysis.

GO enrichment analysis was performed using  $\text{FDR} < 0.05$  as the significant enrichment threshold [18]. Figures 3(a)~3(b) displays the partial results of GO enrichment analysis for common DEGs in AT and ATA groups. Among the 610 significantly enriched GO entries ( $P < 0.05$ ), 102 were related to cell composition (CC), 66 to molecular function (MF), and 442 to biological process (BP). Notably, cell cycle, cell cycle process, mitotic cell cycle, mitotic cell cycle process, and other biological processes played crucial roles in the allicin-induced reversal of Taxol resistance in A549/Taxol cells.

In order to further understand the metabolic pathways and specific biological functions of DEGs, OmicShare tools were used for KEGG enrichment analysis [19].  $P < 0.05$  and  $\text{FDR} < 0.05$  were statistical thresholds of significance, which indicated the pathways were significantly enriched in DEGs. The top 20 pathways were enriched in the analysis of differential gene expression between AT and ATA (Figures 3(c)~3(d)). Cell cycle, Fanconi anemia pathway, oocyte metabolism, homologous recombination,

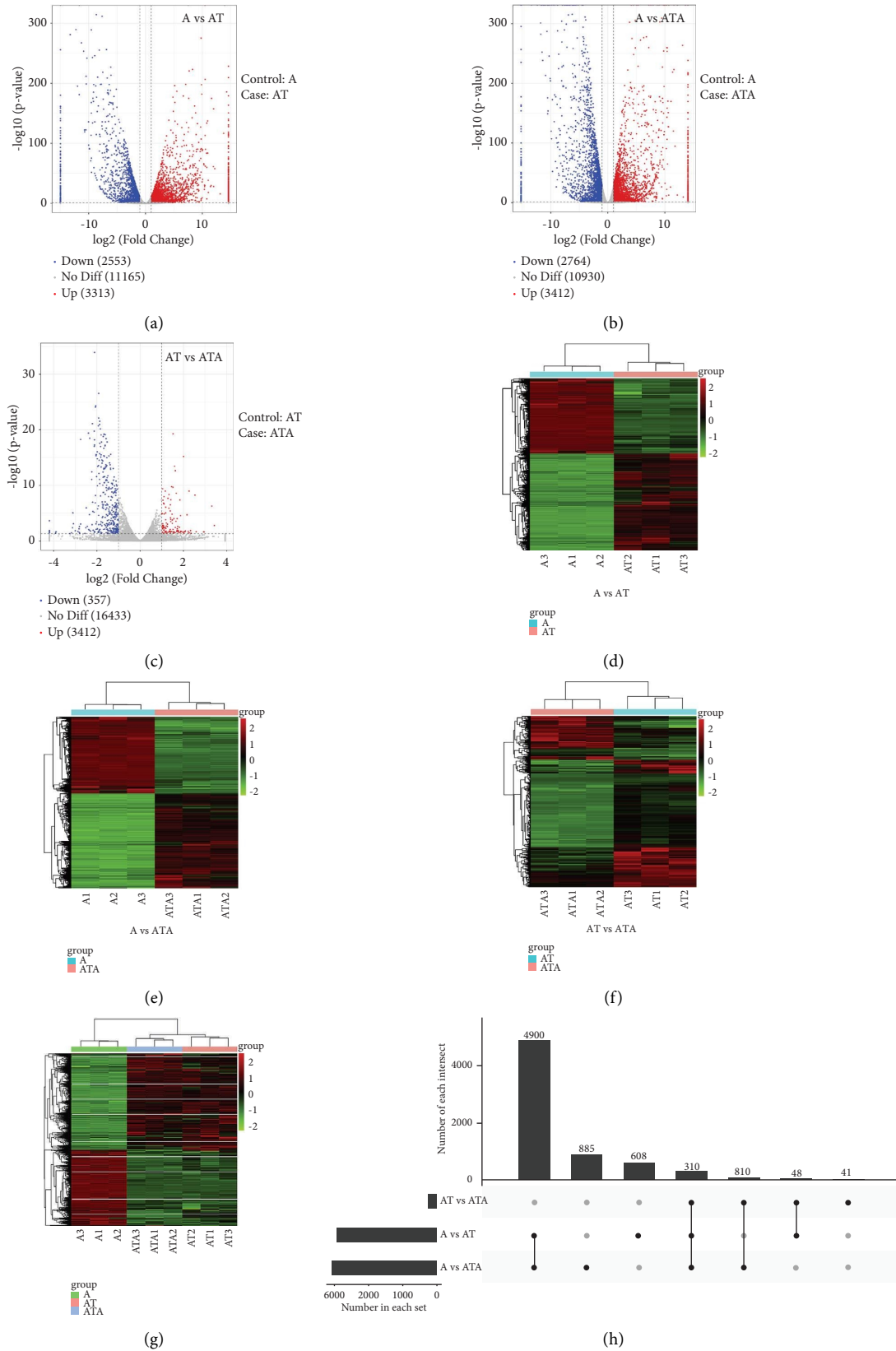


FIGURE 2: Continued.

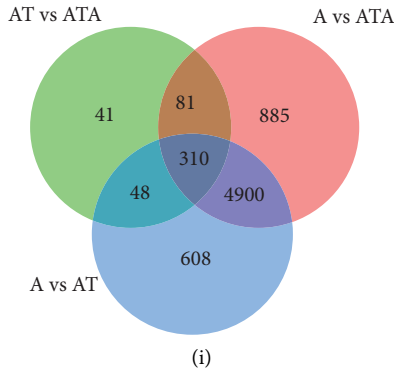


FIGURE 2: The differentially expressed genes (DEGs) between groups ((a~c): the volcano map manifested differentially expressed mRNA; (d~f): the cluster heat map with the differential expression patterns of mRNAs; (g) hierarchical clustering heat map of DEGs in three comparisons; (h) the Upset diagrams of DEGs in three comparisons; (i) the Venn diagrams of DEGs in three comparisons. Note: In the volcano plot, the abscissa was  $\log_2$  (FC) value and the ordinate was  $-\log P$  value, and the significant difference between upregulated and downregulated mRNA was red and blue, respectively. In the heat map, the ordinate represents the probe number and the abscissa represents the sample name; red represents upregulated expression, green represents downregulated expression, and black represents no difference in expression. The significance was indicated by  $P < 0.05$ ).

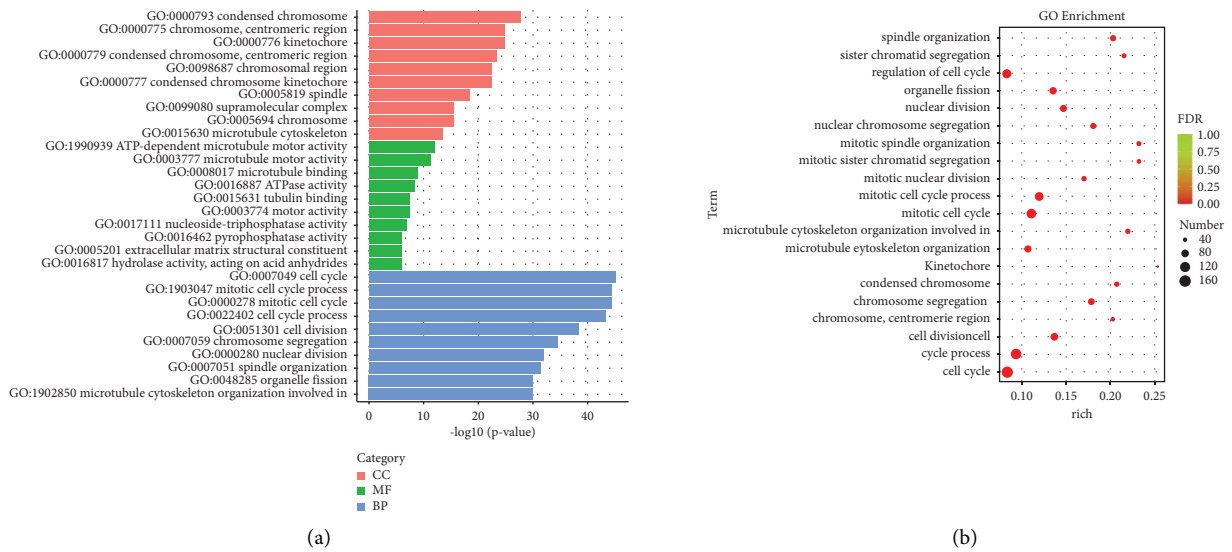


FIGURE 3: Continued.



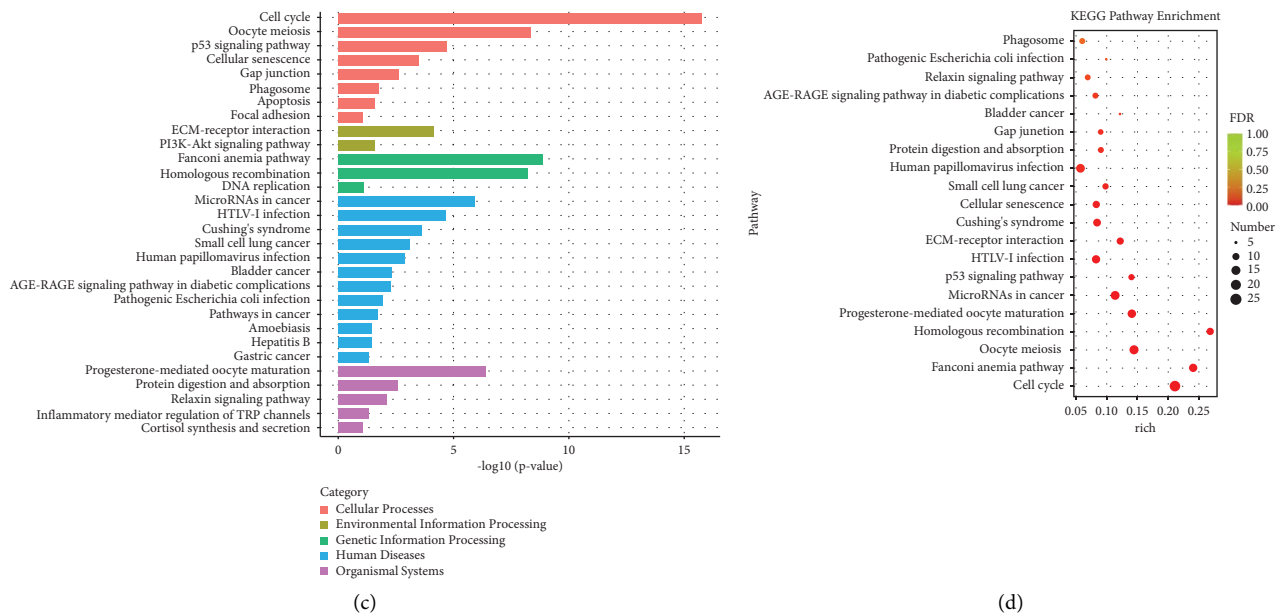


FIGURE 3: The GO and KEGG analysis. (a) Classification of identified genes based on functional annotations using GO analysis are shown for comparisons between AT and ATA; (b) GO enrichment bubble chart of DEGs; (c) functional path analysis of differentially expressed genes between AT and ATA represented by histograms; (d) top 20 pathway enrichment in KEGG pathway analysis.

progesterone-mediated oocyte formation, microRNAs in cancer, p53 signaling pathway, and other signal pathways are enriched, among them, the cell cycle signal pathway was the most significant in the reversal of Taxol resistance by allicin.

**3.4. Protein-Protein Interaction (PPI) Network of DEGs.** PPI analysis was conducted using the STRING database, and the PPI network was visualized in Cytoscape [11]. In the PPI analysis of differential genes between AT and ATA, PPI pairs with a score  $> 0.95$  and  $P < 1.0 \times 10^{-16}$  were screened. The resulting PPI network had 277 nodes, a mean degree of 54.6, and an average local clustering coefficient of 0.667. The top 15 genes based on the degree value included CDK1, CCNA2, BuB1, CCNB1, KIF11, PLK1, CCNB2, CDC20, BUB1B, NDC80, TOP2A, AURKB, ASPM, DLGAP5, and KIF20A (Figure 4). These 15 genes were downregulated in the ATA group compared to the AT group. Biological function evaluation revealed that these genes were mainly involved in cell cycle, oocyte meiosis, and other pathways.

### 3.5. Reversal of Taxol Resistance in Non-Small-Cell Lung Cancer with Allicin In Vitro and In Vivo

**3.5.1. Allicin Reverses Taxol Resistance in A549/Taxol Cells by Arresting G2/M Phase.** According to the analysis results of AT and ATA DEGs, allicin could reverse Taxol resistance by regulating the cell cycle of A549/Taxol cells. Flow cytometry and western blot were used to detect the cell cycle, the results showed that compared with the NC group, A549/Taxol cells treated with  $5 \mu\text{M}$  of allicin combined with Taxol (300 nM) did not have a significant effect on the cell cycle, but 10 and  $20 \mu\text{M}$  of allicin combined with Taxol (300 nM) treatment for 24 h could significantly decrease the proportion of cells in

S phase ( $P < 0.05$ ) and increase the proportion of cells in G2/M phase ( $P < 0.05$ ) with a concentration-dependent manner (Figure 5(a)). A549/Taxol cells treated with allicin (10,  $20 \mu\text{M}$ ) and Taxol (300 nM) exhibited G2/M phase arrest, which prevented mitosis and inhibited cell proliferation.

In order to further clarify the potential mechanism of cell cycle arrest induced by allicin combined with Taxol, we examined the expression level of G2/M phase-related proteins by western blot analysis. CDK1 and cyclin B1 form active heterodimers and participate in the transition of the cell cycle from G2 phase to M phase, after DNA damage, CDK1 activity is regulated by p21, which is the key for cancer cells to enter G2/M phase [20]. Among these CDKs, CDK1 and cyclin B1 could form an active heterodimer, which was involved in the transition of the cell cycle from G2 phase to M phase. After DNA was damaged, CDK1 activity was regulated by p21, which was the key for cancer cells to enter G2/M phase. As shown in Figure 5(b), the expression levels of CDK1 and cyclin B1 in A549/Taxol cells treated with allicin (10,  $20 \mu\text{M}$ ) combined with Taxol were significantly decreased, and the expression levels of p21 were increased in a concentration-dependent manner ( $P < 0.05$ ). These results indicated that G2/M phase arrest of A549/Taxol cells was helpful to induce cell death.

**3.5.2. Allicin Could Significantly Reverse Taxol Resistance in the Orthotopic A549/Taxol Tumor Bearing Nude Mouse Model.** The nude mouse orthotopic tumor model of Taxol-resistant human non-small-cell lung cancer was used to verify the reversal of drug resistance of allicin *in vivo*. During the administration, the changes of body weight and activity ability were observed and recorded daily in each group of mice. The results showed that, as shown in Figures 6(a)–6(c),



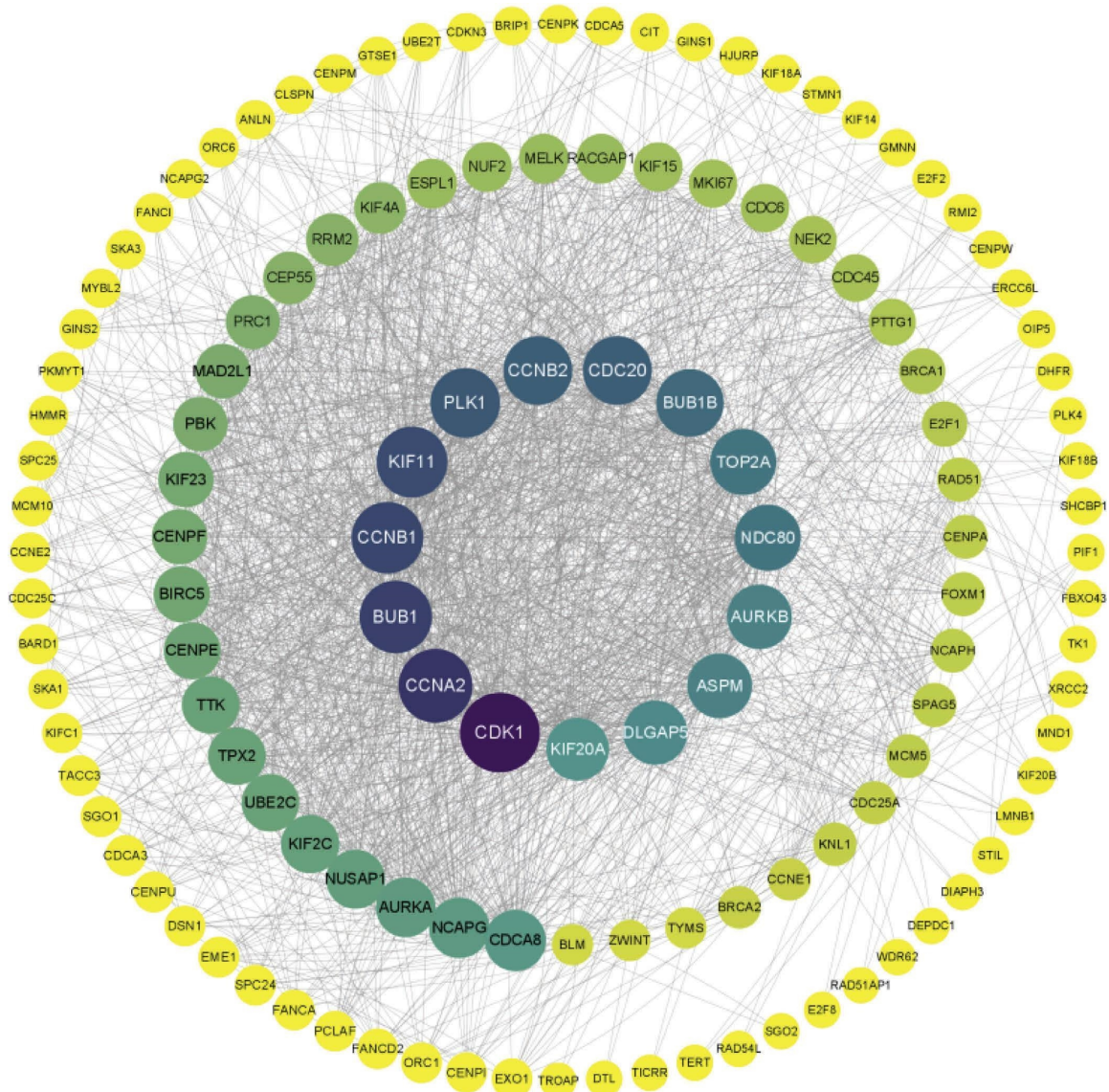
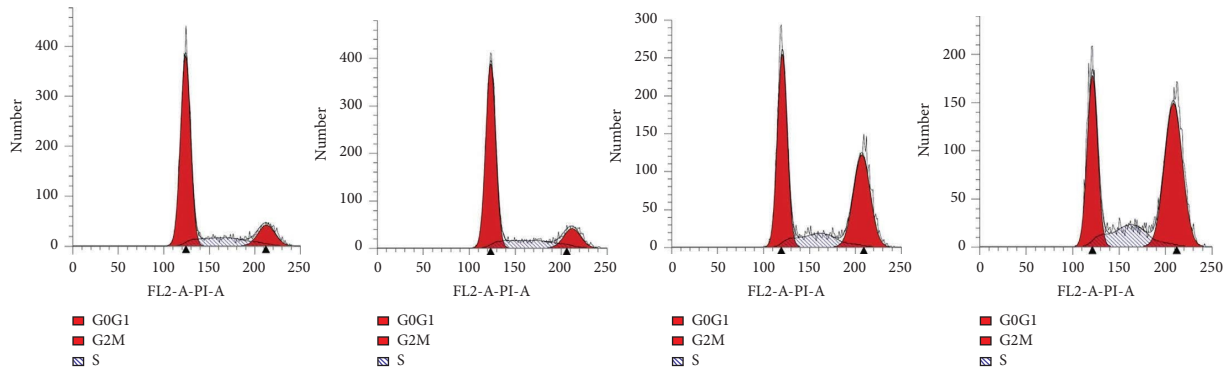


FIGURE 4: The PPI protein interaction network of DEGs in AT group compared with AA group.

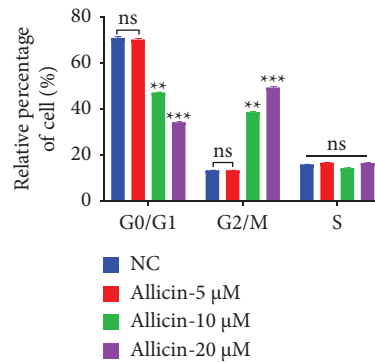
the lung tissue of the normal group mice was smooth and had no pathological changes. Compared with the normal group, the lung tumor of the model, Taxol, or allicin group was significantly enlarged and protruding, and the whole lung surface was uneven, and there were many tumor nodules of different sizes visible to the naked eye on the surface of the lung tissue. However, the tumor growth of allicin combined with the Taxol group was significantly inhibited, and the surface of lung tissue was relatively smooth, and the number of lung tumor nodules was significantly reduced. During the treatment period, the activity and mental state of the tumor-bearing nude mice were observed every day. The mice in each group were normal, and there was no malaise or abnormal behavior. At the same time, according to the body weight of nude mice recorded every day during the treatment period and the body weight change curve drawn, compared with the model group, the body weight of the nude mice in the blank control group and

allicin combined with Taxol showed the steady increase trend, and the body weight of other groups decreased after 9 days of treatment. The results showed that after allicin combined with Taxol treatment, the survival status of mice was improved, and allicin increased the therapeutic effect of Taxol *in vivo*.

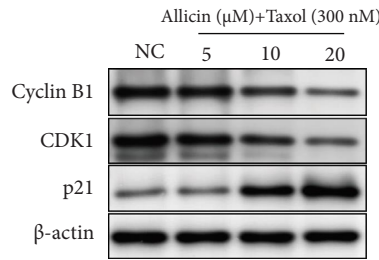
To observe the pathological changes in the lung tissues of tumor-bearing mice, HE staining was performed. Compared with the blank group, the alveoli of the model group and Taxol group were covered by nodules, while the formation rate of pulmonary nodules in the allicin group and the intended combination of Taxol group was slower than that of the model group and Taxol group (Figure 6(e)). It is worth noting that we observed sparse pink cytoplasm and densely stained circular or elliptical vesicular nuclei in tumor cells of the model and Taxol groups. Furthermore, to validate the role of allicin in reversing resistance by blocking the G2/M phase of the cell cycle *in vivo*, we examined the expression



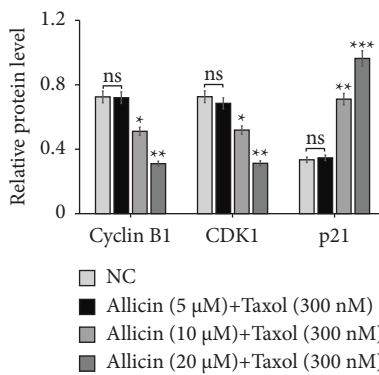
(a)



(b)



(c)



(d)

FIGURE 5: The effect of allicin combined with Taxol on cell cycle arrest in A549/Taxol cells (a) Analysis of cell cycle distribution of A549/Taxol after 24 h treatment with allicin and Taxol by flow cytometry; (b) the expression level of cell cycle related proteins was detected by western blot. The results of relative protein expression were expressed by histogram. Single factor analysis of variance (ANOVA) was used for statistical comparison, and then Dunnett's posttest was used for multiple comparisons ( $n = 3$ ). The data were expressed as mean  $\pm$  SD, \* compared with the control group,  $P < 0.05$ , \*\* $P < 0.01$ , \*\*\* $P < 0.001$ .

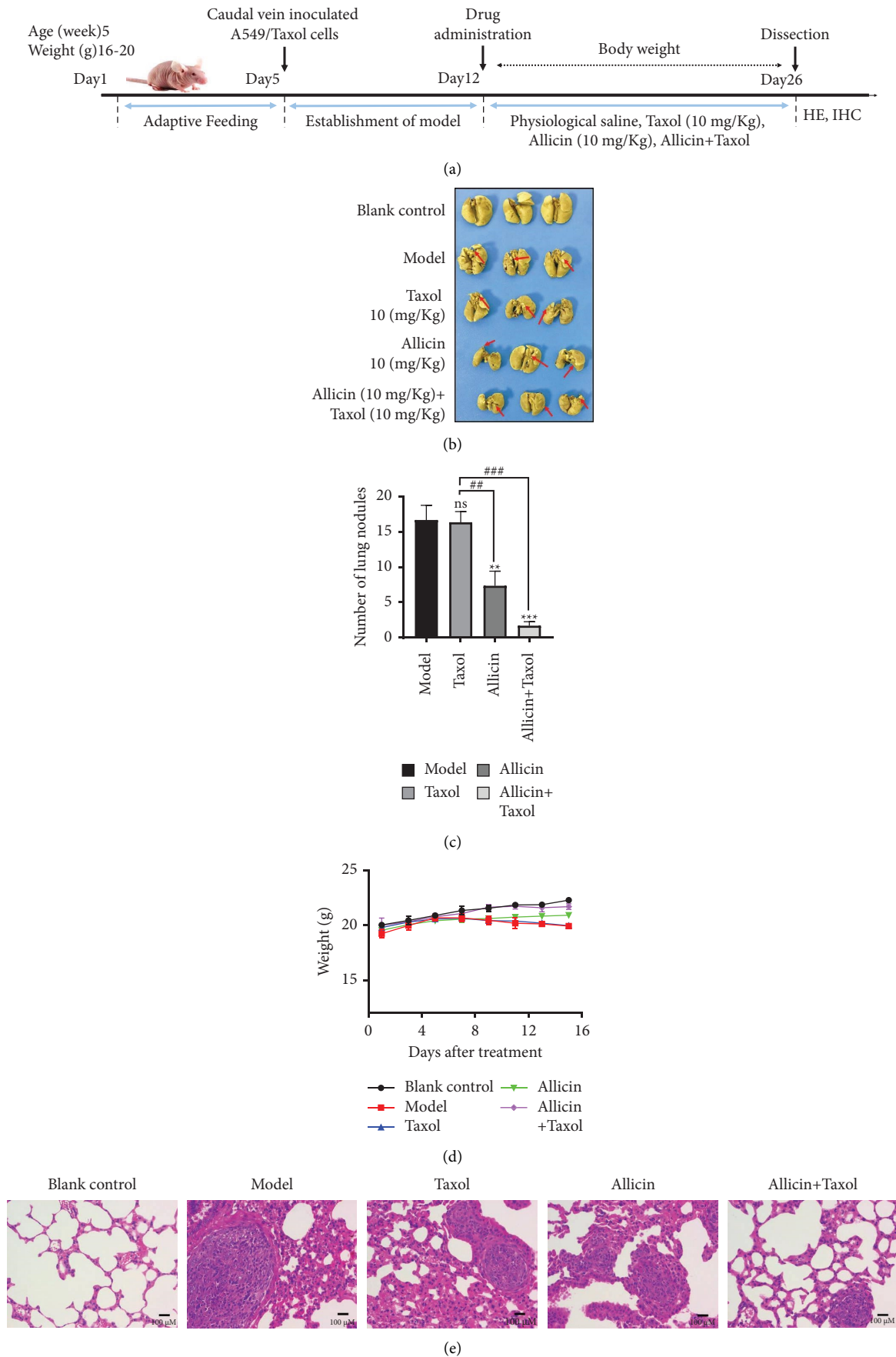
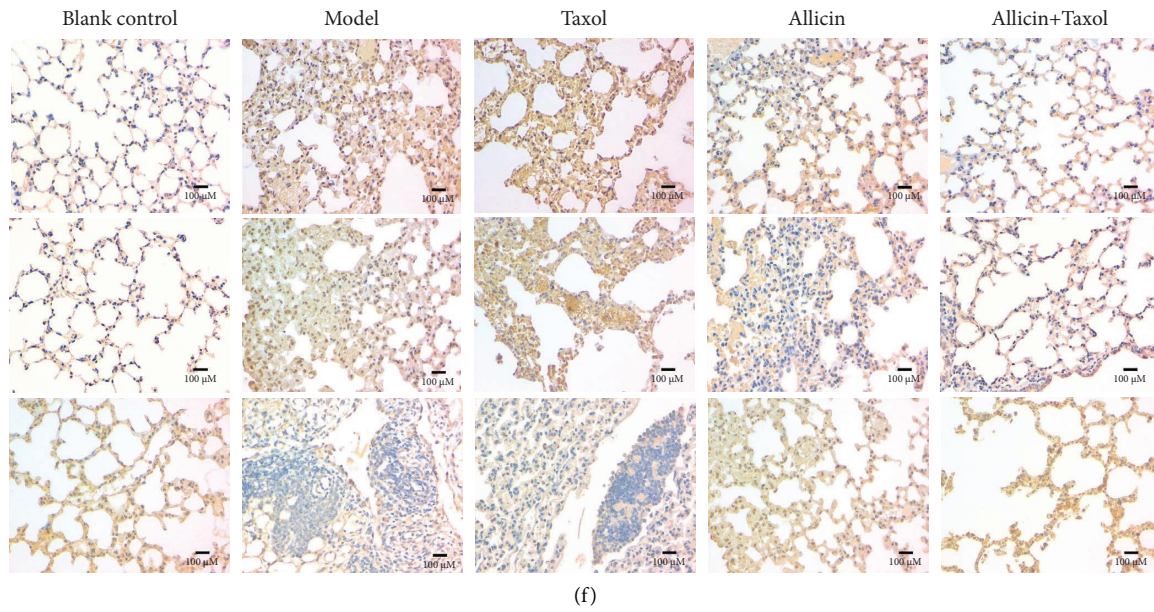


FIGURE 6: Continued.





(f)

FIGURE 6: Allicin combined with Taxol inhibits tumor growth in an orthotopic A549/Taxol nude mice model by tail vein. (a) The schematic figure of tumor modeling nude mice and drug administration. (b) The images of orthotopic A549/Taxol lung samples in nude mice based on the Bouin's staining ( $n = 3$ ). (c) Statistical analysis of the number of lung nodules in mice in each group ( $n = 3$ ). (d) Body weight change curve of nude mice after drug administrations. (e) Hematoxylin and eosin (HE) staining of lung tissues in each group (400 $\times$ ). (f) The expressions of cyclin B1, CDK1, and p21 in lung tissues were detected by immunohistochemistry. Scale bar = 100  $\mu\text{m}$ . The data were expressed as mean  $\pm$  SD, \* compared with the blank control group,  $P < 0.05$ , \*\*  $P < 0.01$ , \*\*\*  $P < 0.001$ ; # compared with the Taxol group,  $P < 0.05$ , ##  $P < 0.01$ , ###  $P < 0.001$ .

levels of cyclin B1, CDK1, and p21 through IHC. Following allicin treatment, there was a downregulation of cyclin B1 and CDK1 expression, while p21 expression was upregulated (Figure 6(f)). This indicates that allicin can reverse resistance by blocking the cell cycle, which is consistent with the *in vitro* results.

#### 4. Discussion

Chemotherapy remains a crucial systemic therapy for preventing tumor metastasis in NSCLC, with Taxol being a commonly used drug. However, drug resistance poses a significant challenge to its efficacy in clinical practice. Increasing drug dosage can lead to severe side effects, prompting research into drug resistance reversal agents and combination therapies to enhance treatment outcomes.

Natural products, such as garlic, have shown promise as potential sources of anticancer agents. Allicin, the main component of garlic, has demonstrated significant anti-proliferative effects on various tumor cells. Studies have revealed that allicin can reduce resistance to 5-Fu in gastric cancer cells, increase sensitivity to 5-Fu in HCC cells, and inhibit resistance to cisplatin in A549 and NCI-H460 cells through different molecular pathways [21]. In our study, we explored the potential of allicin to sensitize and reverse drug resistance to Taxol in A549 cells. We observed that treatment with allicin at  $\text{IC}_{10}$  concentration combined with Taxol significantly inhibited the proliferation of A549/Taxol cells. Furthermore, A549/Taxol cells regained their sensitivity to Taxol in a concentration-time-dependent manner,

indicating that allicin could enhance Taxol's effectiveness and reverse drug resistance. Overall, these findings suggest that allicin holds promise as a potential adjuvant therapy to improve the efficacy of Taxol and overcome drug resistance in NSCLC, contributing to better treatment outcomes for patients.

In order to find the key regulatory genes of Taxol-resistance reversal by allicin, A549 cells, A549/Taxol cells, and A549/Taxol cells treated with allicin for 24 hours were used as the research objects in this study. The gene expression profiles of these cells were analyzed by RNA-Seq technology, and the possible genes and related pathway mechanisms involved in allicin reversal of Taxol resistance in A549 cells were discussed. The study found that the number of common DEGs in the three groups was 310, among them, the top 15 genes CDK1, CCNA2, BuB1, CCNB1, KIF11, PLK1, CCNB2, CDC20, BUB1B, NDC80, TOP2A, AURKB, ASPM, DLGAP5, and KIF20A were the key genes for allicin to reverse Taxol resistance in A549/Taxol cells. The GO enrichment results of DEGs showed that there were 422, 66, and 102 GO enrichment items for BP, MF, and CC, respectively. The enriched entries were mainly related to cell cycle regulation and mitotic cycle regulation. Based on NGS sequencing technology, this study screened DEGs before and after allicin treatment on A549/Taxol cells, and found four major signal pathways: cell cycle pathway, homologous recombination pathway, microRNA pathway in cancer, and p53 signal pathway. The cell cycle pathway with the most significant changes in biological function has been further studied.

Cyclins, protein-dependent kinases, and kinase inhibitors can regulate the cell cycle together, and their abnormal expression will lead to the imbalance of cell cycle [22]. The cell cycle consists of G0/G1 phase, S phase, and G2/M phase. Cyclin B1 is a M phase cyclin, which is expressed from S phase and gradually disappears after reaching the peak in G2/M phase; the activation of CDK1 depends on cyclin B1, and the activated CDK1 can promote cells to enter M phase from G2 phase. In many studies, CDK1 has been overexpressed in many malignant tumors and found to be closely related to the drug resistance of 5-Fu, oxaliplatin, sorafenib, cisplatin and other chemotherapy drugs [23–25]. In addition, cyclin B1, as one of the main regulatory genes of G2/M restriction point of the cell cycle, inhibition of cyclin B1 could reduce the production of cyclin B1/CDK1 complex, arrest cells in G2/M phase, and reverse drug resistance or increase drug sensitivity. As a cyclin kinase inhibitor, p21 can play a negative regulatory role in the cell cycle after binding to CDKs, and participate in the biological processes of tumor genesis, development and drug resistance [26]. In our study, it showed that allicin could induce apoptosis in tumor cells by arresting them at the G2/M phase of the cell cycle through multiple gene targets. Allicin inhibits the protein expression of CycE and CycA genes, reducing the phosphorylation of the Rb protein by cyclins, and preventing the separation of transcription factors E2F1 and Dp-1, thus inhibiting the transcription of proteins required for the S phase. Allicin can also affect the expression of genes such as E2F1, E2F2, and E2F3. Allicin also reduces the expression of the cdc gene family, reducing the synthesis of cell division control proteins, DNA replication licensing factor Mcm5, origin recognition complex subunits ORC1 and Orc6, thereby inhibiting S phase DNA activation and indirectly inhibiting DNA biosynthesis. During the G2 to M phase transition, allicin affects the cell cycle protein-dependent kinase CDK1, as well as CycA, CycB, and the checkpoint serine/threonine kinase Bub1, leading to the arrest of tumor cell growth and division, inhibiting the proliferation of Taxol-resistant A549 cells, and inducing apoptosis.

In this study, we observed that the proliferation and migration of Taxol resistant A549 cells were significantly enhanced; the expression of CDK1 in A549/Taxol cells was the highest, and the expression of CDK1 in A549/Taxol cells after allicin treatment was significantly reduced. It was further found that allicin could induce cell cycle arrest in the G2/M phase by regulating cyclin B1/CDK1 and p21 and inhibit A549/Taxol cell proliferation, migration, and its sensitivity to Taxol. To sum up, this study screened the DEGs of A549, A549/Taxol, and A549/Taxol cells treated with allicin based on NGS sequencing technology and found that cell cycle pathway, homologous recombination pathway, microRNA pathway in cancer, p53 signal pathway, and other signal pathways were closely related to Taxol resistance. It was preliminarily concluded that CDK1, CCNA2, BuB1, CCNB1, PLK1, CCNB2, CDC20, and BUB1B were the key genes in allicin reversing Taxol resistance in A549 cells, which provided a theoretical basis for expanding the application of allicin.

However, the number of samples in this study was small, and the preliminary verification was only conducted through *in vitro* experiments. The conclusions were limited, and the research conclusions need to be verified by *in vivo* and *in vitro* experiments; the mechanism of Taxol resistance in lung cancer is complex, and a single target or signaling pathway has limitations in the treatment. Therefore, it was particularly important to explore the relationship between multiple signaling pathways in reversing drug resistance, which could provide a novel strategy for the clinical prevention and treatment of non-small-cell lung cancer drug resistance and improve the cure rate and survival rate of patients.

## 5. Conclusions

RNA transcriptome sequencing revealed that the cell cycle pathway, homologous recombination pathway, microRNA pathway, p53 signaling pathway, and other signaling pathways were closely related to Taxol resistance in A549/Taxol cells. This study proved that allicin could reverse the Taxol resistance in A549/Taxol cells *via* targeting the cell cycle pathway. Allicin could induce G2/M phase cycle arrest, inhibit the proliferation and migration of A549/Taxol cells, and reverse the resistance of NSCLC cells to Taxol by downregulating the expression of cyclin B1/CDK1 and upregulating the expression of p21. Allicin may eventually serve as a chemotherapeutic treatment for tumors that can reverse medication resistance, according to the evidence. It is necessary to continue developing allicin's therapeutic approach to overcome Taxol resistance in NSCLC cells.

## Data Availability

The datasets generated during and/or analyzed during the current study are available from the corresponding authors on reasonable request.

## Ethical Approval

The animal study was reviewed and approved by Medical Ethical Committee of the General Hospital of Northern Theater Command.

## Conflicts of Interest

The authors declare that they have no conflicts of interest.

## Authors' Contributions

Xudong Gao contributed to the design of experiments, methodology, verification, software, formal analysis, manuscript writers, and funding acquisition. Ramesh kumar Santhanam investigated data analysis and he also checked the grammar of the manuscript. Zeng Huang and Mingyue Liu contributed substantially to cell culture and cytotoxicity assay, data acquisition, statistical analysis, and data interpretation. Shanbo Hou and Aigang Song provided support in the revisions, data updates, and discussions of our manuscript, while they also made adjustments to the image

quality and layout in the manuscript. Tianshu Ren supervised the manuscript and provided software, instruments, and reagents. Qingchun Zhao has made an important contribution to the supervision of the manuscript. All authors have read and approved the final manuscript.

## Acknowledgments

This work was supported by the grant from the Liaoning Provincial Natural Science Foundation of Doctoral Research Foundation (Grant no. 2022-BS-033) and the Shenyang Science and Technology Plan Project (Grant no. 22-321-33-19).

## References

- [1] Y. Wu, J. Xie, H. Wang, S. Hou, and J. Feng, "Circular RNA hsa\_circ\_0011298 enhances Taxol resistance of non-small cell lung cancer by regulating miR-486-3p/CRABP2 axis," *Journal of Clinical Laboratory Analysis*, vol. 36, no. 5, pp. e24408–e24412, 2022.
- [2] B. Xu, H. Cheng, K. Li et al., "Carboplatin and nab-paclitaxel chemotherapy with or without atezolizumab as front-line management for treatment-naïve metastatic nonsquamous non-small cell lung cancer with PD-L1 staining: a retrospective study," *Journal of Cancer Research and Clinical Oncology*, vol. 148, no. 11, pp. 3029–3038, 2022.
- [3] J. Liu, D. Ding, F. Liu, and Y. Chen, "Rhein inhibits the progression of chemoresistant lung cancer cell lines via the stat3/snail/MMP2/MMP9 pathway," *BioMed Research International*, vol. 2022, Article ID 7184871, 8 pages, 2022.
- [4] M. Liu, C. Xu, X. Qin et al., "DHW-221, a dual PI3K/mTOR inhibitor, overcomes multidrug resistance by targeting P-glycoprotein (P-gp/ABCB1) and akt-mediated FOXO3a nuclear translocation in non-small cell lung cancer," *Frontiers in Oncology*, vol. 12, no. May, pp. 873649–873720, 2022.
- [5] C. Zhang, J. Xie, X. Li et al., "Alliin alters gut microbiota and gene expression of colonic epithelial tissues," *Journal of Food Biochemistry*, vol. 43, no. 4, Article ID e12795, 2019.
- [6] P. Wongsu, P. Bhuyar, and J. Müller, "Assessment of phenolic profile, allicin content, and inhibitory potential against  $\alpha$ -amylase and  $\alpha$ -glucosidase on conventional and organic garlic (*Allium sativum* L.)," *European Food Research and Technology*, vol. 249, pp. 1–13, 2023.
- [7] X. Yang, S. Bai, J. Wu et al., "Antifungal activity and potential action mechanism of allicin against trichosporon asahii," *Microbiology Spectrum*, vol. 11, no. 3, pp. e0090723–23, 2023.
- [8] E. Catanzaro, D. Canistro, V. Pellicioni, F. Vivarelli, and C. Fimognari, "Anticancer potential of allicin: a review," *Pharmacological Research*, vol. 177, Article ID 106118, 2022.
- [9] M. S. Nadeem, I. Kazmi, I. Ullah, K. Muhammad, and F. Anwar, "Allicin, an antioxidant and neuroprotective agent, ameliorates cognitive impairment," *Antioxidants*, vol. 11, no. 1, p. 87, 2022.
- [10] W. Li, Y. Li, H. Zhang et al., "HOTAIR promotes gefitinib resistance through modification of EZH2 and silencing p16 and p21 in non-small cell lung cancer," *Journal of Cancer*, vol. 12, no. 18, pp. 5562–5572, 2021.
- [11] C. Huang, H. Luo, Y. Huang et al., "Aurkb, chek1 and nek2 as the potential target proteins of scutellaria barbata on hepatocellular carcinoma: an integrated bioinformatics analysis," *International Journal of General Medicine*, vol. 14, pp. 3295–3312, 2021.
- [12] L. Y. D. Almeida, F. Moreira, G. A. S. D. Santos et al., "FASN inhibition sensitizes metastatic OSCC cells to cisplatin and paclitaxel by downregulating cyclin B1," *Oral Diseases*, vol. 29, no. 2, pp. 649–660, 2021.
- [13] Y. Sun, P. Wu, Y. Sun et al., "Lycorine possesses notable anticancer potentials in on-small cell lung carcinoma cells via blocking Wnt/ $\beta$ -catenin signaling and epithelial-mesenchymal transition (EMT)," *Biochemical and Biophysical Research Communications*, vol. 495, no. 1, pp. 911–921, 2018.
- [14] W. Ding, C. Chen, J. Li, X. Geng, H. Zhang, and Y. Sun, "Quercus acutissima Carruth. root extract triggers apoptosis, autophagy and inhibits cell viability in breast cancer cells," *Journal of Ethnopharmacology*, vol. 289, Article ID 115039, 2022.
- [15] C. Yi, J. Liu, W. Deng et al., "Macrophage elastase (MMP12) critically contributes to the development of subretinal fibrosis," *Journal of Neuroinflammation*, vol. 19, no. 1, p. 78, 2022.
- [16] B. Andrade Barbosa, S. D. van Asten, J. W. Oh et al., "Bayesian log-normal deconvolution for enhanced in silico microdissection of bulk gene expression data," *Nature Communications*, vol. 12, no. 1, pp. 6106–6113, 2021.
- [17] D. Chen, H. Wang, and X. Cai, "Curcumin interferes with sepsis-induced cardiomyocyte apoptosis via TLR1 inhibition," *Revista Portuguesa de Cardiologia*, vol. 42, no. 3, pp. 209–221, 2023.
- [18] Z. Xin, Y. Cai, L. T. Dang et al., "MonaGO: a novel gene ontology enrichment analysis visualisation system," *BMC Bioinformatics*, vol. 23, no. 1, pp. 69–16, 2022.
- [19] T. K. Wang, S. Xu, Y. Fan et al., "The synergistic effect of proanthocyanidin and HDAC inhibitor inhibit breast cancer cell growth and promote apoptosis," *International Journal of Molecular Sciences*, vol. 24, no. 13, Article ID 10476, 2023.
- [20] S. Sunada, H. Saito, D. Zhang, Z. Xu, and Y. Miki, "Cdk1 inhibitor controls G<sub>2</sub>/M phase transition and reverses DNA damage sensitivity," *Biochemical and Biophysical Research Communications*, vol. 550, no. 6518, pp. 56–61, 2021.
- [21] P. Khakbaz, R. Panahzadeh, M. A. Vatankeh, and N. Najafzadeh, "Allicin reduces 5-fluorouracil-resistance in gastric Cancer cells through modulating MDRI, DKK1, and WNT5A expression," *Drug Research (Stuttg)*, vol. 71, no. 8, pp. 448–454, 2021.
- [22] R. Roskoski, "Cyclin-dependent protein serine/threonine kinase inhibitors as anticancer drugs," *Pharmacological Research*, vol. 139, pp. 471–488, 2019.
- [23] J. Shang, Y. D. Xu, Y. Y. Zhang, and M. Li, "Long noncoding RNA OR3A4 promotes cisplatin resistance of non-small cell lung cancer by upregulating CDK1," *European Review for Medical and Pharmacological Sciences*, vol. 23, no. 10, pp. 4220–4225, 2019.
- [24] J. Li, X. Zhi, X. Shen et al., "Depletion of UBE2C reduces ovarian cancer malignancy and reverses cisplatin resistance via downregulating CDK1," *Biochemical and Biophysical Research Communications*, vol. 523, no. 2, pp. 434–440, 2020.
- [25] Y. Zhu, K. Li, J. Zhang, L. Wang, L. Sheng, and L. Yan, "Inhibition of cdk1 reverses the resistance of 5-fu in colorectal cancer," *Cancer Management and Research*, vol. 12, pp. 11271–11283, 2020.
- [26] C. Yang, F. Li, J. Ma et al., "Evaluation of anti-cancer potency of silibinin on murine renal carcinoma RenCa cells in an animal model with an intact immune system," *Anti-Cancer Drugs*, vol. 31, no. 8, pp. 785–791, 2020.